Published in final edited form as:

Plant J. 2020 July ; 103(2): 752–768. doi:10.1111/tpj.14769.

The Arabidopsis transcription factor AINTEGUMENTA orchestrates patterning genes and auxin signaling in the establishment of floral growth and form

Beth A. Krizek[1,*], **Ivory C. Blakley**[2], **Yen-Yi Ho**[3], **Nowlan Freese**[2], **Ann E. Loraine**[2]

[1]Department of Biological Sciences, University of South Carolina, Columbia, SC

[2]Department of Bioinformatics and Genomics, University of North Carolina at Charlotte, Charlotte, NC

[3]Department of Statistics, University of South Carolina, Columbia, SC

Summary

Understanding how flowers form is an important problem in plant biology, as the human food supply depends on flower and seed production. Flower development also provides an excellent model for understanding how cell division, expansion and differentiation are coordinated during organogenesis. In the model plant *Arabidopsis thaliana*, floral organogenesis requires AINTEGUMENTA (ANT) and AINTEGUMENTA-LIKE6 (AIL6)/PLETHORA3 (PLT3), two members of the Arabidopsis AINTEGUMENTA-LIKE/PLETHORA (AIL/PLT) transcription factor family. Together, ANT and AIL6/PLT3 regulate aspects of floral organogenesis including floral organ initiation, growth, identity specification, and patterning. Previously, we used RNA-Seq to identify thousands of genes with disrupted expression in *ant ail6* mutant flowers, indicating that ANT and AIL6/PLT3 influence a vast transcriptional network. However, the immediate downstream targets of ANT and AIL6/PLT3 in flowers are unknown. To identify direct targets of ANT regulation, we performed a RNA-Seq time course experiment in which we induced ANT activity in transgenic plants bearing an ANT-glucocorticoid receptor fusion construct. In addition, we performed a ChIP-Seq experiment that identified ANT binding sites in developing flowers. These experiments identified 200 potential ANT target genes based on their proximity to ANT binding sites and differential expression in response to ANT. These 200 candidate target genes were involved in functions such as polarity specification, floral organ development, meristem development and auxin signaling. In addition, we identified several genes associated with lateral organ growth that may mediate ANT's role in organ size control. These results reveal new features of the ANT transcriptional network by linking ANT to previously unknown regulatory targets.

[*]Corresponding author: Tel: +1 803-777-1876, krizek@sc.edu.

Author Contributions

BAK and AEL designed the research. BAK carried out the experiments. BAK, ICB, YYH, NF and AEL performed the data analyses. BAK wrote the manuscript. All authors edited the manuscript.

Conflict of Interest

The authors declare that they have no conflicts of interest.

Keywords

Arabidopsis thaliana; flower development; AINTEGUMENTA (ANT); AINTEGUMENTA-LIKE (AIL)/PLETHORA (PLT); RNA-Seq; ChIP-Seq; organ polarity; organ growth; auxin signaling

Introduction

Flowers supply fruits, seeds and grains to the human diet and are a subject of fascination for their beauty and morphological diversity. Molecular genetic studies in Arabidopsis have identified many regulatory factors that control the initiation and subsequent development of flowers. Flower primordia arise in the periphery of the inflorescence meristem at sites of auxin maxima, during the reproductive phase of the plant life cycle (Benkova *et al.* 2003, Heisler *et al.* 2005, Reinhardt *et al.* 2003). At these sites, AUXIN RESPONSE FACTOR5/MONOPTEROS (ARF5/MP) upregulates the expression of *LEAFY* (*LFY)* and two *AINTEGUMENTA-LIKE/PLETHORA* (*AIL/PLT*) genes: *AINTEGUMENTA* (*ANT*) and *AINTEGUMENTA-LIKE6* (*AIL6*)/*PLETHORA3* (*PLT3*) to specify these primordia as flowers and promote their outgrowth (Yamaguchi *et al.* 2013). Within flower primordia, floral organ primordia are initiated at defined positions within whorls and subsequently adopt one of four fates according to the ABCE model [reviewed in (Krizek and Fletcher 2005)]. Class A and E gene activities in whorl one specify sepal identity; class A, B and E gene activities in whorl two specify petal identity; class B, C and E gene activities in whorl three specify stamen identity, and class C and E gene activities in whorl four specify carpel identity.

Most class A, B, C and E floral organ identity genes encode MADS domain transcription factors that act in higher order protein complexes to regulate gene expression (Smaczniak *et al.* 2012). Genomic studies on these transcription factors have begun to reveal the gene regulatory networks that control the development of each floral organ type (Kaufmann *et al.* 2009, Kaufmann *et al.* 2010, O'Maoiléidigh *et al.* 2013, Wuest *et al.* 2012). These studies indicate that floral organ identity proteins regulate a large number of genes throughout floral organ development with distinct genes being regulated at different stages of organ development [reviewed in (Stewart *et al.* 2016, Yan *et al.* 2016)]. Direct regulatory targets include other transcription factors as well as genes involved in plant hormone signaling pathways and developmental processes such as pattern formation and morphogenesis. Furthermore, the floral organ identity proteins appear to repress the expression of genes that specify a leaf developmental program (O'Maoiléidigh *et al.* 2013).

Genetic studies have uncovered multiple roles for *ANT* and *AIL6/PLT3* during the initiation and subsequent development of floral organ primordia. *ANT* and *AIL6/PLT3* promote the initiation of floral organ primordia at defined positions within the floral meristem and also prevent premature differentiation of both primordial and floral meristem cells (Krizek 2009, Krizek and Eaddy 2012). *ANT* and *AIL6/PLT3* function is required for proper expression of the class B and C floral organ identity genes *APETALA3* (*AP3)* and *AGAMOUS* (*AG)*, respectively and consequently the elaboration of petal and stamen fates (Krizek 2009). *ANT* and *AIL6/PLT3* also regulate the growth of developing floral organs, thus contributing to

morphogenesis and the attainment of correct organ size (Elliott *et al.* 1996, Klucher *et al.* 1996, Krizek 1999, Mizukami and Fischer 2000). Despite their well-established importance in many facets of flower development, we currently know very little about the downstream target genes that are activated or repressed by ANT and AIL6/PLT3. Without this knowledge, we lack understanding of the biological processes regulated by these transcription factors that contribute to the sculpting of each floral organ type.

A genomic study comparing the transcriptomes of wild type and *ant ail6* double mutants identified thousands of differentially expressed (DE) genes, consistent with the numerous roles of ANT and AIL6/PLT3 in floral organogenesis and the severe phenotypic consequences of losing *ANT* and *AIL6/PLT3* functions (Krizek *et al.* 2016). This experiment suggested that ANT and AIL6/PLT3 functions are intimately coupled within a vast transcriptional network regulating floral organogenesis. To distinguish between short-term and longer-term consequences of loss of *ANT* and *AIL6/PLT3* activities, we have utilized more focused genomic studies. We performed two complementary experiments: RNA-Seq analysis of floral buds at two, four, and eight hours after induction of ANT activity, and ChIP-Seq analysis of stage 6/7 flowers. Together, these studies identified 200 genes that are both differentially expressed after ANT induction and are bound by ANT and are thus likely to be direct targets of ANT regulation. Our experiments suggest that ANT controls floral organogenesis through direct regulation of growth and patterning genes as well as auxin responses.

Results

RNA-Seq identifies genes differentially expressed after activation of ANT-GR

To identify direct targets of ANT regulation, we created a line of transgenic plants containing an inducible form of ANT in which the ligand binding domain of the glucocorticoid receptor (GR) was fused to the coding region of *ANT*. In this system, the GR domain blocks migration of the ANT-GR fusion partner into the nucleus, rendering it incapable of activating or repressing the expression of target genes. Applying the steroid dexamethasone (dex) causes a conformational change in GR that permits entry of ANT-GR into the nucleus, where it can bind to target promoters and regulate gene expression. Applying dex to *35S:ANT-GR* inflorescences led to the production of larger flowers and caused male sterility, similar to the phenotypes observed in *35S:ANT* inflorescences (Figure S1) (Krizek 1999, Yamaguchi *et al.* 2013). This established that the ANT-GR line contained inducible ANT activity that could be triggered by application of dex.

We performed a time course experiment using the *35S:ANT-GR* line in which floral buds were collected two, four, and eight hours following dex treatment or treatment with a solvent only (mock) negative control. Whole inflorescences corresponding to floral buds stage 1–12 were collected as four matched pairs of treatment and control samples and processed for RNA sequencing. Following sequencing and alignment to the Arabidopsis reference genome, each sample yielded between 13 and 29 million aligned fragments, which were then analyzed for differential expression. Using a false discovery rate (FDR) of 0.05, we identified 1,195 genes that were DE at one or more time points (Data S1). More DE genes were present at four (746) and eight hours (609) post treatment as compared with two hours

(324) (Figure 1A). The log2 fold change (logFC) values of the DE genes ranged from 3.15 to −1.80. There were 106 genes that were DE at all three time points. Approximately equal numbers of upregulated (836) and downregulated (843) genes were identified.

To visualize gene expression changes over time, we developed an interactive R Shiny app (called “Show gene expression”) that plots individual gene expression data over the time course of the experiment (available at https://bitbucket.org/lorainelab/inducible-ant-rna-seq/) (Figure S2A–D). After launching the Shiny App in the RStudio application, users can generate plots showing expression of a gene of interest after entering its gene identifier. Gene expression can be visualized as “Sample RPKM” with individual treatment and time points selected, “Group RPKM” which averages the four replicates for each sample, or “Expression over time”, in which the data can be visualized with lines, points or arrows that indicate up or down regulation between the control and treated samples. The “gene info” tab provides a link to TAIR (The Arabidopsis Information Resource) for further information about the gene. We used this app to investigate expression of candidate target genes and explore their functions.

DE genes were enriched in terms associated with development and hormone physiology

We used enrichment analysis to identify Gene Ontology (GO) and KEGG functional annotation categories overrepresented among the 1,195 DE genes. We further investigated individual gene functions using TAIR for members of these categories.

Many DE genes had functions related to lateral organ development, consistent with ANT’s role as a regulator of organogenesis. These included: leaf formation (GO:0010338), polarity specification of adaxial/abaxial axis specification (GO:0009944), and stamen development (GO:0048443) (Figure 1B). Seven genes that regulate lateral organ polarity were differentially expressed (Table S1). These genes included three *YABBY* genes [*CRABS CLAW (CRC)*, *YAB3*, *YAB5*], one class III HD-ZIP gene [*PHABULOSA* (*PHB*)], one *KANADI* gene (*KAN2*) as well as *ASYMMMETRIC LEAVES 1* (*AS1*) and *BLADE ON PETIOLE 1* (*BOP1*). Thus both adaxial (*PHB, AS1, BOP1*) and abaxial (*CRC, YAB3, YAB5, KAN2*) genes were identified as potential targets of ANT regulation. The identification of genes regulating adaxial/abaxial axis specification is consistent with previous genetic work suggesting that ANT contributes to organ polarity (Nole-Wilson and Krizek 2006). Leaf development GO category genes include several genes regulating organ growth including *KLUH (KLU/CYP78A5*), *GROWTH REGULATING FACTORS* (*GRF3*, *GRF6*, *GRF8*) and *ANGUSTIFOLIA3/GRF1-INTERACTING FACTOR1 (AN3/GIF1)*.

Several genes with known roles in floral organ development were DE. These included floral organ identity genes *APETALA1* (*AP1*), *APETALA2* (*AP2*), and *SEPALLATA3* (*SEP3*), as well as genes that function in later aspects of stamen development [*SQUAMOSA PROMOTER-BINDING PROTEIN-LIKE 8* (*SPL8*), *EXCESS MICROSPOROCYTES1* (*EMS1*)] and carpel development [*SPATULA* (*SPT*), *CRC*, *STRUBBELIG* (*SUB*)] (Table S1).

In addition to genes involved in lateral organ development, seven DE genes involved in meristem maintenance (GO:0010073), were identified: *CORYNE* (*CRN*), *BARELY ANY*

MERISTEM 3 (*BAM3*), *CLAVATA3 INSENSITIVE RECEPTOR KINASE 4* (*CIK4*), *MINI ZINC FINGER 2* (*MIF2*), and *FANTASTIC FOUR 1, 2, 3* (*FAF1, FAF2, FAF3*) (Table S1). This suggests that ANT has a role in meristems maintenance in addition to its role in lateral organ development, consistent with genetic work showing the importance of *ANT* and *AIL6/PLT3* in preventing premature differentiation of floral meristem cells (Krizek and Eaddy 2012).

Many hormone-related functions were enriched in the DE genes (Data S2) suggesting that ANT function is closely linked with multiple aspects of hormone physiology. These GO terms included: negative regulation of cytokinin-activated signaling pathway (GO: 0080037), regulation of jasmonic acid mediated signaling pathway (GO:2000022), regulation of auxin mediated signaling pathway (GO:0010928), jasmonic acid mediated signaling pathway (GO:0009867), gibberellin mediated signaling pathway (GO:0010476), auxin-activated signaling pathway (GO:0009734)], hormone biosynthesis [(indoleacetic acid biosynthetic process (GO:000009684), jasmonic acid biosynthetic process (GO:0009695)], hormone transport [auxin efflux (GO:0010315), and auxin transport (GO:0060918)] (Figure 1B). Additional analysis using the KEGG pathway framework also found links with cytokinin, auxin, and gibberellin hormone signaling pathways (Figure S3). DE genes associated with the synthesis/metabolism, transport, signaling and response for cytokinin, auxin, gibberellin, abscisic acid and jasmonic acid are shown in Table S2. These results suggest that ANT plays roles in the metabolism of auxin and jasmonic acid (and perhaps cytokinin and gibberellin) while also influencing signaling pathways downstream of cytokinin, auxin, gibberellin, abscisic acid and jasmonic acid. Our earlier RNA-Seq investigation of *ant ail6* double mutants inflorescences previously linked ANT function with auxin biosynthesis and JA signaling but not cytokinin or gibberellin signaling (Krizek *et al.* 2016).

ChIP-Seq identifies ANT genomic binding sites in stage 6/7 flowers

To identify genome-wide ANT binding sites, we performed chromatin immunoprecipitation in combination with next generation sequencing (ChIP-Seq). For these studies, we used a transgenic line in which an *ANT-VENUS* gene fusion was expressed under the control of the *ANT* promoter in the *ant* mutant background. Fusion of ANT with VENUS, a rapidly folding variant of YELLOW FLUORESCENT PROTEIN (YFP), allows immunoprecipitation of DNA bound to ANT by a commercially available antibody against GREEN FLUORESCENT PROTEIN (GFP). The transgene fully rescued the *ant-4* mutant phenotype as assayed by petal measurements and floral organ counts, indicating that the ANT-VENUS fusion protein has full ANT activity (Tables S3, S4). The *ANT:ANT-VENUS ant-4* line was crossed into a genetic background in which flower development can be synchronized (i.e. *AP1:AP1-GR ap1 cal*) (O'Maoiléidigh *et al.* 2015), allowing us to collect large numbers of flowers of the same developmental stage. Inflorescences from two biological replicates of *AP1:AP1-GR ap1 cal* and *AP1:AP1-GR ap1 cal ANT:ANT-VENUS ant-4* were harvested five days after dex treatment when they are composed of stage 6/7 flowers.

In our ChIP-Seq experiment, we identified 1,113 ANT binding peaks in stage 6/7 flowers using visual analytics and the Integrated Genome Browser (IGB). These peaks were associated with 1,081 unique genes (Data S3). Almost half of the peaks (48%) are present upstream of the gene near the transcriptional start site (TSS) with the remaining peaks either overlapping the start of transcription (18%), within the gene (15%), overlapping the end of transcription (5%), downstream of the gene (14%) or encompassing the gene (1%) (Figure 2A, B).

Genes associated with ANT binding sites include regulators of polarity specification, floral organ development and meristem development

To gain insight into the set of genes associated with ANT ChIP-Seq peaks, we performed a GO enrichment analysis (Data S4; Figure 3). Several of the identified GO terms were the same or similar to those identified in the ANT-GR RNA-Seq experiment. Within the biological process GO category, a number of developmental terms were identified that relate to adaxial/abaxial polarity, floral organ development and meristem development including the following: polarity specification of adaxial/abaxial axis (GO:0009944), floral organ formation (GO:0048449), meristem determinacy (GO:0010022), meristem initiation (GO:0010014), plant ovule development (GO:0048481), stamen development (GO:0048443), and regulation of flower development (GO:0009909) (Figure 3A). Other overrepresented developmental GO biological process terms include: stomatal complex morphogenesis (GO:0010103), cell fate specification (GO:0001708), and leaf development (GO:0048366) (Figure 3A). Two hormone-related overrepresented GO biological process terms are the following: response to gibberellin (GO:0009739) and auxin-activated signaling pathway (GO:0009734), which were also identified in the RNA-Seq experiment (Figure 3A). However, several other hormone-related GO terms such as those related to cytokinin and JA signaling identified in the RNA-Seq experiment were not enriched in the ChIP-Seq experiment.

The biological process GO term “positive regulation of transcription, DNA-templated” (GO:0045893) was also overrepresented, which suggests that ANT regulates the expression of other transcription factors (Figure 3A). This is also supported by the identification of the following enriched molecular function GO terms: RNA polymerase II regulatory region DNA binding (GO:0001012), DNA-binding transcription factor activity (GO:0003700), and sequence-specific DNA binding (GO:0043565) (Figure 3B). Another enriched molecular function GO term was protein homodimerization activity (GO:0042803) (Figure 3B).

The enriched cellular component GO term glyoxysome (GO:0009514) was also identified (Figure 3B). This category includes two enzymes, isocitrate lyase (ICL) and malate synthase (MS), specific to the glyoxylate cycle which occurs in glyoxysomes.

200 DE genes are bound by ANT and likely direct targets of ANT regulation

The most likely direct targets of ANT regulation are genes that are both bound by ANT and are differentially expressed in response to changes in ANT activity. There were 200 genes common between the set of RNA-Seq DE genes and the set of ChIP-Seq bound genes (Figure 4A; Data S5). While the total set of DE genes (1,195) consists of slightly less

upregulated genes (523) than downregulated genes (672), a much larger number of upregulated genes (154) are associated with ANT binding peaks as compared with downregulated genes (46).

GO term enrichment analysis on this set of 200 genes identifies several GO terms similar to or the same as those identified for the entire set of ANT ChIP-Seq associated genes (Data S6; Figure 4). In particular, three terms were enriched in both sets: polarity specification of adaxial/abaxial axis (GO:0009944), regulation of transcription, DNA-templated (GO:0006355), and DNA-binding transcription factor activity (GO:0003700) (Figure 4). Five polarity genes were identified: *PHB*, *BOP1*, *AS1*, *KAN2* and *YAB3* (Table 1). Other enriched GO terms were the following: gynoecium development (GO:0048467), floral organ development (GO:0048437), meristem development (GO:0048507), phyllome development (GO:0048827), and response to hormone (GO:0009725). Floral organ development genes include those involved in specifying floral organ identity (*AP1, AP2, SEP3*), regulating cellular differentiation (*EMS1, SPL8*) and controlling morphogenesis (*SUB, SPT*) (Table 1). Nine auxin genes were part of the hormone responses category including those involved in biosynthesis (*TAA1*), signaling (*AFB2, ARF6, ARF11, ARF18, IAA3/SHY2, IAA27, PAP2*) and responses (*SAUR50, SAUR14*) (Table 2). To confirm our RNA-Seq and ChIP-Seq results, we selected eight genes from this set of 200. The selected genes were not previously known to be regulated by ANT and were associated with several different biological processes. The eight genes included two polarity genes *KAN2* and *PHB*; two hormone signaling genes *BES1/BZR1 HOMOLOG 4* (*BEH4*), *REPRESSOR OF GA* (*RGA*); the reproductive organ development gene *SPL8*; and three genes that regulate lateral organ growth: *AN3/GIF1*, *XYLOGLUCAN ENDOTRANSGLUCOSYLASE/ HYDROLASE 9* (*XTH9*) and *SMALL RUBBER PARTICLE PROTEIN2* (*SRP2*) (Table 1).

We examined the expression of these eight genes in an independent batch of mock and dex treated *35S:ANT-GR* inflorescences. To determine if activation of these target genes required *de novo* protein synthesis, we included inflorescences treated with the protein synthesis inhibitor cycloheximide (chx). Inflorescences were collected four hours after the respective treatment. Similar changes in gene expression in inflorescences treated with dex +chx versus chx alone as compared with those treated with dex versus mock support direct regulation of the gene by ANT. Seven of the eight DE genes showed expression changes independent of protein synthesis in *35S:ANT-GR* inflorescences (Figure 5). The lone exception was *SRP2* which showed similar expression levels in chx and dex+chx samples (Figure 5). Thus, SRP2 may not be a direct target of ANT regulation, although it is possible that the use of whole inflorescences in the RT-qPCR experiment obscured developmental stage-specific regulation of this gene by ANT in stage 6/7 flowers.

ChIP-qPCR experiments performed on these eight genes with an independent batch of ChIP DNA gave results that are similar to those seen by ChIP-Seq (Figure 6, Figure S4). ANT binds to regions upstream or overlapping the 5’ UTR (*PHB, RGA, SPL8, AN3/GIF1, XTH9, SRP2*) or within the gene body (*KAN2*, *BEH4*) in stage 6/7 flowers. No enrichment was observed in *AP1:AP1-GR ap1 cal* inflorescences lacking *ANT:ANT-VENUS*. ANT binds to genomic regions of both upregulated (*KAN2, PHB, BEH4, RGA, AN3/GIF1, XTH9, SRP2)* and a downregulated (*SPL8*) gene.

DNA sequence motif analyses of ChIP-Seq peaks

In previous work using SELEX, we identified the *in vitro* DNA binding motif of ANT (Nole-Wilson and Krizek 2000). To determine whether ANT binding peaks contain DNA sequences with similarity to this motif, we mapped putative ANT binding sites on a genome-wide level using the FIMO program from the MEME software suite (Grant *et al.* 2011). We then compared the position of the FIMO predicted sites to both the ChIP-Seq peaks and to a set of randomized peaks of the same size. 66.7% of the ChIP-Seq peaks and 43.8% of the randomized peaks overlapped a FIMO site. Thus, ChIP-Seq peaks were more likely than randomized peaks to contain a FIMO predicted ANT binding site. However, nearly a third of the ChIP-Seq peaks did not contain a FIMO predicted ANT binding site.

We used MEME-ChIP from the MEME Suite to perform *de novo* motif discovery (Machanick and Bailey 2011). Our analysis used the DAP-Seq database for motif discovery which includes several AIL/PLT binding sites but not that of ANT (O'Malley *et al.* 2016). MEME-ChIP identified seven motifs with an e-value of 1.00E-10 or lower (Table 3). Two of these motifs: MEME-1 (HNNNHGGCACRNWTH) and MEME-3 (RCACRRWWHYCRAKG) were similar to the PLT1 and AIL6/PLT3 DAP-Seq binding motifs, respectively (Table 3; Figure 7A). The PLT1 and AIL6/PLT3 binding sites consisted of a fairly long sequence with several conserved residues near each end of the site and less conserved nucleotides in the center. The ANT SELEX determined *in vitro* binding motif is similar to both of these sites (Figure 7A) (Nole-Wilson and Krizek 2000). The MEME-1 motif had similarity to the first conserved part of AIL/PLT sites, while the MEME-3 motif had similarity to both conserved parts of AIL/PLT sites (Figure 7A). Thus, the identification of MEME-1 and MEME-3 motifs in ANT binding peaks suggests that the *in vivo* binding specificity of ANT resembles that determined *in vitro* but with less conservation at several positions within the motif. Interestingly, in some MEME-1 sites, a second motif was identified at a conserved distance from the MEME-1 motif and resembled the second half of AIL/PLT binding sites (Figure S5).

MEME-ChIP identified several other enriched motifs in ANT binding peaks. These had similarity to the binding sites of other transcription factors. Two such motifs, MEME-2 (YTYTBTCTYTYTYTY) and DREME-2 (ARAGARAR), resembled the binding sites of BASIC PENTACYSTEINE (BPC) transcription factors (Table 3, Figure 7B). These transcription factors bind GA repeat sequences present in many plant promoters. Recently BPC proteins were shown to bind to Polycomb response elements (PREs) and interact with components of Polycomb repressive complex 2 (PRC2) to mediate the silencing of gene expression by PRC2 (Xiao *et al.* 2017). Two additional motifs, MEME-5 (GYRRRTSCCACGTG), and DREME-1 (CGWGSC), resembled the binding sites of basic HELIX LOOP HELIX (bHLH) transcription factors (Table 3, Figure 7C). In particular the identified motifs most closely match the DAP-Seq binding sites of BIG PETAL (BPE)/ bHLH31 and PHYTOCHROME INTERACTING FACTOR7 (PIF7).

The ANT ChIP-Seq gene set exhibited limited overlap with those from AP1, JAG and PLT2

To investigate where ANT acts within the hierarchy of known flower development regulators, we compared the set of genes bound by ANT to genes bound by other

transcription factors involved in flower development as determined by ChIP-chip or ChIP-Seq experiments. We compared ANT with the floral meristem identity protein LFY, the floral organ identity proteins AP1, AP3, PI, AG and SEP3, the growth regulator JAGGED (JAG), and AUXIN RESPONSE FACTOR 3/ETTIN (ARF3/ETT) which regulates gynoecium development (O'Maoiléidigh *et al.* 2013, Pajoro *et al.* 2014, Schiessl *et al.* 2014, Simonini *et al.* 2017, Winter *et al.* 2011, Wuest *et al.* 2012). Fisher's exact tests were performed using the R package GeneOverlap (Shen and Sinai 2019). GeneOverlap also calculates the Jaccard index to assess the overlap of two gene lists. A Jaccard index of 0 indicates no similarity between the gene lists while a value of 1 indicates the lists are identical. Comparisons between the gene set of ANT with gene sets from LFY, AP3, PI, AG, SEP3, and ETT each gave a Jaccard index of 0.1 while the comparison between ANT and JAG and that between ANT and AP1 gave a Jaccard index of 0.2 (Figure S6). This degree of overlap is much less than that observed among the floral organ identity proteins AP3, PI and AG which exhibit Jaccard indices of 0.4 or 0.5 (Figure S6). JAG also showed a Jaccard Index of 0.2 with the floral organ identity proteins SEP3, AP1, and PI.

We also compared the set of ANT ChIP-Seq bound genes with genes bound by two other AIL/PLT transcription factors: PLT2, which specifies stem cell identity in the root and regulates shoot phyllotaxy and BABYBOOM (BBM), which promotes somatic embryogenesis (Aida *et al.* 2004, Boutilier *et al.* 2002, Prasad *et al.* 2011). The PLT2 ChIP-Seq experiment utilized roots and the BBM ChIP-Seq experiment used somatic embryos (BBM) (Horstman *et al.* 2015, Santuari *et al.* 2016). The comparison with PLT2 gave a Jaccard index of 0.2 while that with BBM gave a Jaccard index of 0.1. It is interesting that ANT showed more overlap with the related PLT2 transcription factor, which primarily functions in roots, versus most non-related transcription factors that regulate floral organ identity.

ANT may repress *SPL8* to promote petal growth

One of the 200 likely direct targets of ANT regulation is *SPL8*, a gene that acts in micro- and megasporogenesis (Unte *et al.* 2003). *spl8* mutants produce slightly thinner flowers than wild type and have stamens with smaller anthers and shorter filaments (Unte *et al.* 2003). *SPL8* mRNA levels are reduced in dex-treated *35S:ANT-GR* inflorescences, and ANT binds to its 5' UTR (Figures 5, 6). This suggests that ANT can directly repress *SPL8* expression. To investigate a possible genetic interaction between *ANT* and *SPL8*, we generated *ant-4 spl8–1* double mutants. *ant-4 spl8–1* flowers exhibit a partial suppression of the petal growth defects of *ant-4* (Figure 8A). Petal width and petal area are larger in *ant-4 spl8–1* flowers as compared with *ant-4* flowers (Figure 8B). This finding suggests that *SPL8* acts as a repressor of petal growth in the *ant-4* background and that one means by which ANT promotes petal growth is through downregulation of *SPL8*. A role in petal development has not previously been noted for *SPL8* although the gene is expressed in the margins of petals in stage 8 flowers (Unte *et al.* 2003). The molecular mechanism by which *SPL8* may repress petal growth in *ant* mutants is not clear as *spl8–1* mutants have smaller petals than those in wild type flowers (Figure S7).

Discussion

ANT is a key regulator of floral organ growth that acts in a redundant manner with *AIL6/PLT3* to regulate the initiation, identity and patterning of floral organs (Elliott *et al.* 1996, Klucher *et al.* 1996, Krizek 1999, Krizek 2009, Mizukami and Fischer 2000). Using transcriptional profiling and genome-wide mapping of ANT binding sites, we identified 200 genes that both responded to changes in ANT activity and were bound by ANT. This set of genes included auxin signaling genes as well as genes that specify floral organ identity, establish polarity, regulate growth, and promote cell differentiation. Thus our work begins to reveal the molecular means by which ANT regulates growth and patterning during floral organogenesis and identifies candidate direct target genes in the larger transcriptional network surrounding ANT.

Our studies reveal that ANT can act directly as both a transcriptional activator and transcriptional repressor. The set of 200 likely direct targets of ANT regulation include both upregulated and downregulated genes. More upregulated genes (154) are associated with ANT binding peaks compared with downregulated genes (46), suggesting that ANT primarily acts as a transcriptional activator. While our work suggests that ANT binds *in vivo* to DNA sequences with similarity to the *in vitro* determined ANT binding motif, not all ANT binding peaks contain an AIL/PLT-like site, as defined by the MEME discovered MEME-1 and MEME-3 motifs. Thus, ANT may bind directly to other DNA sequences and/or be recruited to different DNA sites via interaction with other transcription factors. The identification of DNA binding motifs of BPC and bHLH transcription factors within ANT peaks suggests that ANT may be recruited to some DNA sites via interaction with other classes of transcription factors.

A comparison of the set of genes bound by ANT with those bound by other floral regulators did not reveal strong overlap with any other gene set as measured by the Jaccard index. This is consistent with ANT having functions that are distinct from transcription factors specifying floral meristem or floral organ identity. One limitation of these comparisons is the different tissues used in these studies. The LFY, JAG and ETT experiments were performed with whole inflorescences while the SEP3, AP1, AP3, PI, and AG used stage 5 flowers. Among floral regulators tested, the highest overlap of ANT was seen with AP1 and JAG. JAG is a regulator of floral organ shape, which suggests that ANT and JAG may regulate some common target genes mediating floral organ growth. We also observed higher overlap with the root stem cell regulator PLT2 despite the different tissues used in the ChIP-Seq experiments (stage 6/7 flowers versus seedlings). The similar DNA binding specificities of ANT and PLT2 may result in the regulation of some common targets despite the distinct morphologies and functions of roots and flowers.

ANT directly regulates genes involved in auxin signaling

Genomic studies in the root have shown that AIL/PLT transcription factors directly regulate genes involved in auxin biosynthesis and transport. Our studies here imply that ANT directly regulates auxin signaling in developing flowers (Santuari *et al.* 2016, Zúñiga-Mayo *et al.* 2019). While our RNA-Seq experiment suggested that ANT could regulate other hormone signaling pathways including cytokinin, gibberellin, and JA, the DE genes in these

categories were not bound by ANT and are thus likely to be indirect targets of ANT regulation. However, it is also possible that these genes may be bound by ANT at a different stage of flower development, since the RNA-Seq experiment utilized floral buds of stage 1–12 while the ChIP-Seq experiment utilized stage 6/7 buds.

Auxin is linked to many aspects of flower development including floral organ initiation, primordium growth, stamen filament elongation, pollen maturation and gynoecium patterning, several of which overlap with ANT function (Cheng *et al.* 2006, Marsch-Martînez and de Folter 2016). Patterning of distinct tissues and cell types within the gynoecium appears to involve complex transcriptional networks and the precise distributions of hormones, particularly auxin and cytokinin (Zúñiga-Mayo *et al.* 2019). Within the gynoecium, *ANT* acts redundantly with several other genes including *REV* to promote the development of the carpel marginal meristem, a meristematic region within the medial domain of the ovary that gives rise to multiple tissues including the placentae, ovules and transmitting tract (Azhakanandam *et al.* 2008, Krizek 2009, Liu *et al.* 2000, Nole-Wilson and Krizek 2006). In *ant rev* double mutants, medial domain development is disrupted and there is partial loss of the carpel marginal meristem (Nole-Wilson *et al.* 2010). These defects are associated with reduced expression of the auxin biosynthetic enzyme *TAA1* in stage 7 gynoecium (Nole-Wilson *et al.* 2010). We found that ANT induction activated *TAA1* expression and that ANT bound to *TAA1*. These results suggest that ANT may be a direct regulator of *TAA1* in this tissue. Mutation of the ANT binding site within the *TAA1* gene would help to reveal whether ANT is required for expression of this gene within the gynoecium.

ANT directly regulates genes that specify floral organ identity

Three of the 200 likely direct targets of ANT regulation were floral organ identity genes: the class A genes *AP1* and *AP2* and the class E gene *SEP3*. *AP1* was downregulated after ANT induction while *AP2* and *SEP3* were upregulated (Table 1). Expression of *AP1*, *AP2* and *SEP3* is initiated early in flower development (stage 1 for *AP1* and *AP2* and stage 2 for *SEP3*) and maintained in developing flowers (Jofuku *et al.* 1994, Mandel *et al.* 1992, Mandel and Yanofsky 1998). Thus, the binding of ANT to the regulatory regions of these genes in stage 6/7 flowers may reflect a role in maintaining (*AP2, SEP3*) or limiting (*AP1*) expression in later stages of flower development.

The combined activities of class A and E genes specify sepal identity which is not disrupted in *ant* single mutants or *ant ail6* double mutants. However, in combination with class B genes, class A and E genes also contribute to the specification of petal identity in the second whorl. Petals are not present in *ant ail6* flowers and expression of the class B gene *AP3* is reduced (Krizek 2009, Krizek *et al.* 2016). While we detected binding of ANT to the regulatory regions of *AP3* in stage 6/7 flowers (Dataset S3), we failed to observe statistically significant differential expression of *AP3* following induction of ANT activity. Failure to detect a significant difference between treatment and control samples in any time point was not due to low *AP3* expression, as *AP3* was highly expressed in these samples. Instead, this negative result may have been due to the timing of the floral stage examined, the bulk nature

of the tissue collected, or because ANT requires some other unknown factor to alter *AP3* expression.

ANT directly regulates genes acting later in floral organogenesis that control growth and differentiation

We found that ANT directly regulates genes that act in the elaboration of organ size and shape and the differentiation of distinct cell types. We showed that ANT binds to two genes involved in stamen development: *EXCESS MICROSPOROCYTES1* (*EMS1*) and *SPL8*. EMS1 encodes a leucine-rich repeat receptor kinase that is required for tapetal cell differentiation (Huang *et al.* 2016, Zhao *et al.* 2002) and *SPL8* encodes an SPB-box transcription factor that is required for the normal development of anther sporogenic tissue (Unte *et al.* 2003, Xing *et al.* 2010). Both *EMS1* and *SPL8* were downregulated after induction of ANT activity, consistent with a role for ANT in inhibiting differentiation in early stages of floral organogenesis (Krizek and Eaddy 2012).

Several known regulators of lateral organ growth were identified in the set of 200 DE genes bound by ANT. These were *KLU*, *GRF8*, *AN3/GIF1*, *XTH9*, and *SRP2* which act as growth-promoting genes and *KIP-RELATED PROTEIN 4* (*KRP4)* which acts as a growth repressor (Table 1) (Anastasiou *et al.* 2007, Bemis and Torii 2007, Hyodo *et al.* 2003, Kim *et al.* 2016, Kim *et al.* 2003, Kim and Kende 2004). *GRF8*, *AN3/GIF1*, *XTH9* and *SRP2* were upregulated after ANT induction suggesting they mediate ANT's role in promoting organ growth. Furthermore, *AN3/GIF1* and *XTH9*, have largely overlapping expression patterns with *ANT* which is consistent with ANT acting as an activator of these genes (Figure S8) (Hyodo *et al.* 2003).

The identification of members of the GRF/GIF pathway (GRF8, AN3/GIF) as potential targets of ANT regulation is interesting, as GRFs and their miRNA regulator *miR396* are key regulators of growth in many plant tissues [reviewed in (Liebsch and Palatnik 2020)]. In the root, GRF/GIF complexes repress *AIL/PLT* expression in transit-amplifying cells to promote proliferation of these cells, while PLT1 and PLT2 activate *miR396* within the root stem cell niche to repress *GRF* expression and maintain stem cell identity (Rodriguez *et al.* 2015). The miR396-GRF/GIF module also controls floral organ growth and meristematic competence within reproductive organs, but a connection with AIL/PLT function has not been described (Lee *et al.* 2014, Lee *et al.* 2018). *ant an3* double mutants exhibit more severe defects in leaf growth than either single mutant but there was no enhancement of the carpel marginal meristem defects within the gynoecium (Lee *et al.* 2014). Extensive genetic redundancies in the *AIL/PLT*, *GRF* and *GIF* gene families may complicate interpretation of these results (Lee *et al.* 2014). Future studies will need to address whether AIL/PLT might directly regulate *GRF/GIF* expression or act indirectly through *miR396* in the carpel marginal meristem and whether *AIL/PLT* genes are targets of GRF/GIF regulation.

ANT may promote organ growth through direct regulation of polarity genes

Seven genes associated with lateral organ polarity were identified in our RNA-Seq experiment, of which five genes (*PHB, BOP1, AS1, KAN2*, and *YAB3)* were also next to an ANT binding site (Table 1). The differentially expressed genes included both upregulated

and downregulated genes. We found ANT binding sites near or within four other genes that were not detected as differentially expressed. These included adaxial genes *REVOLUTA (REV)* and *BOP2* and the abaxial genes *KAN2* and *FILAMENTOUS FLOWER (FIL)*. The ANT binding peaks upstream of *FIL* and *YAB3* overlapped an *in vitro* defined ANT binding site (Nole-Wilson and Krizek 2006).

Previous genetic work has suggested a role for ANT in lateral organ polarity. While *ant* single mutants do no show defects in organ polarity, mutations in *ANT* combined with mutations in *FIL* produce plants with smaller leaves that exhibit polarity defects on both the adaxial and abaxial surfaces of leaves (Nole-Wilson and Krizek 2006). *ant fil yab3* triple mutants exhibit even more severe defects in leaf polarity and growth, and *YAB3* and *FIL* expression is reduced in *ant ail6* double mutants (Krizek *et al.* 2016, Nole-Wilson and Krizek 2006). Polarity defects were also observed in *ant fil* floral organs and these defects were associated with reduced expression of *PHB* (Nole-Wilson and Krizek 2006). Together, these data suggest that ANT regulates organ polarity through regulation of both adaxial and abaxial-specifying genes. Since the juxtaposition of adaxial and abaxial cell types is required for outgrowth of the leaf lamina, our work suggests that one mechanism by which ANT controls lateral organ growth is through direct regulation of polarity genes to establish distinct adaxial and abaxial domains within developing lateral organ primordia (Yamaguchi *et al.* 2012).

Overall, the work described here reveals that ANT can directly regulate the expression of target genes involved in various aspects of flower development including floral organ identity, polarity, growth and cellular differentiation. Furthermore, our findings connect ANT function with several hormone pathways that may provide positional information for growth and patterning events during flower development.

Experimental Procedures

Plant materials, growth conditions, genotyping and treatments

35S:ANT-GR plants were grown on a soil mixture of Fafard 4P:perlite:vermiculite (8:1:1) in 16 hour days at a light intensity of approximately 160 micromol/m^2/s at 20°C. *ANT:ANT-VENUS ant-4 AP1:AP1-GR ap1 cal* inflorescences were grown on a soil mixture of Fafard 4P:perlite:vermiculite (8:1:1) in 24 hour days at a light intensity of approximately 160 micromol/m^2/s at 20°C. *ant-4* and *spl8–1* were grown on a soil mixture of Fafard 4P:perlite:vermiculite (8:1:1) in 16 hour days at a light intensity of approximately 160 micromol/m^2/s at 22°C. *ant-4 spl8–1* double mutants were identified by genotyping for *ant-4* and *spl8–1* as described previously (Krizek 2009, Unte *et al.* 2003). *35S:ANT-GR* plants for RNA-Seq and RT-qPCR were treated by pipetting a mock (0.1% ethanol + 0.015% Silwet), dex (10μM dexamethasone +0.015% Silwet), chx (10μM cycloheximide + 0.015% Silwet + 0.1% ethanol), or dex+chx (10μM dexamethasone + 10μM cycloheximide + 0.015% Silwet) solution onto the inflorescences. *AP1:AP1-GR ap1 cal* and *AP1:AP1-GR ap1 cal ANT:ANT-VENUS ant-4* plants for ChIP-Seq and ChIP-qPCR were treated by pipetting a dex (10μM dexamethasone +0.015% Silwet) solution onto the inflorescences.

RNA-Seq

35S:ANT-GR inflorescences containing unopened floral buds (flowers stages 1–12) were collected in four batches at each time point (two, four and eight hours after treatment) consisting of two flats per batch, where dexamethasone was applied to one flat and a mock treatment was applied to the other flat. RNA was extracted from inflorescences using Trizol following the manufacturer's instructions with cleanup and DNase treatment on a RNeasy column (Qiagen). Sequencing libraries were prepared from four biological replicates using TruSeq Stranded mRNA Sample preparation kit (Illumina) and sequenced on the Illumina HiSeq 2500 producing 100 base single-end reads. Sequence reads were aligned to the reference *Arabidopsis thaliana* genome (version TAIR9, released June 2009) using tophat and bowtie2. Reads per gene were counted using featureCounts. Read counts were analyzed using the edgeR software. Differentially expressed genes were identified using an additive linear model with adjustment for batch (flat) effects. Source code for differential expression analysis is available in the project "git" repository https://bitbucket.org/lorainelab/inducible-ant-rna-seq/. Gene Ontology analyses were performed with AmiGO 2 (http://amigo.geneontology.org/amigo).

RT-qPCR

RNA was isolated as described above for RNA-Seq. First strand complementary DNA (cDNA) synthesis was performed using Quanta qScript cDNA SuperMix (Quanta BioSciences) following the manufacturer's instructions. qPCR was performed on a BioRad CFX96 using PerfeCTa SYBR Green FastMix for iQ (Quanta BioSciences) and primers listed in Table S5. Data analyses were carried out as described previously (Krizek and Eaddy 2012). Two biological replicates were analyzed for each experiment.

ChIP-Seq and ChIP-qPCR

Chromatin immunoprecipitation was performed similarly to that described in (Yamaguchi *et al.* 2014) with the same buffers and solutions. Approximately 600mg of inflorescence tissue consisting of stage 6/7 flowers from *AP1:AP1-GR ap1 cal* and *ANT:ANT-VENUS ant-4 AP1:AP1-GR ap1 cal* plants was collected five days after dex treatment into a 2 ml tube filled with 1.5ml cold 1x PBS on ice. The PBS was then removed and replaced with 10mls of room temperature 1% methanol-free formaldehyde (Thermo Scientific) in 1xPBS and 0.015% Silwet L-77 for 15 mins at room temperature. During this time, the tissue was vacuum infiltrated three times for two minutes each time. The fixative was removed and crosslinking stopped with the addition of 10mls of 0.125M glycine and incubated for 5 mins. During this time, the tissue was vacuum infiltrated once for two mins. The tissue was rinsed three times with 10mls cold 1x PBS while on ice, dried briefly on paper towels, frozen in liquid nitrogen, and stored at −80°C. The tissue was ground in liquid nitrogen and 2.5ml nuclei extraction buffer with protease inhibitors and beta-mercaptoethanol was added. The samples were filtered twice through Miracloth and centrifuged at 10,000g for 5 mins at 4°C. The pellet was resuspended in 107 μl of nuclei lysis buffer and left on ice for 30 mins with occasional stirring with a pipet tip. 893 μl of ChIP dilution buffer without Triton X-100 was added to bring the volume to 1 ml. The sample was loaded into a milliTUBE 1ml AFA Fiber tube (Covaris) and chromatin shearing was performed with a Covaris M220 Focused ultra-

sonicator (14 cycles of 75% peak power, 5 duty factor, 200 cycles/burst at 7°C). After sonication, 200 µl of ChIP dilution buffer with Triton X-100 and 53 µl of 22% Triton X-100 was added to each sample. The samples were centrifuged twice at 12,000g for 10 mins at 4°C. The sample was pre-cleared by adding 50 µl of Dynabeads-Protein A and incubating for 2 hours at 4°C on a tube rotator. The sample was removed using a magnetic stand and transferred into a 1.5 ml low adhesion tube. A 12.5 µl sample was removed as the Input sample. 50 µl of GFP (Invitrogen A6455) coated Dynabeads was added to each sample and incubated for 4 hours at 4°C.The samples were washed twice (5 mins each at 4°C) with the following four cold wash buffers: low salt wash buffer, high salt wash buffer, 250mM LiCl buffer, 0.5x TE. Immunoprecipitated DNA was eluted from the Dynabeads by the addition of 50 µl of Nuclei Lysis Buffer and a 30 minute incubation at 65°C on a Thermomixer. The elution was repeated a second time and the samples combined. Crosslinks were reversed by the addition of 6 µl of 5M NaCl to the ChIP samples and an overnight incubation at 65°C. 87.5 µl of Nuclei Lysis buffer and 6 µl of 5M NaCl was added to the input samples followed by overnight incubation at 65°C. The input and ChIP DNA was purified using Qiagen PCR purification kit. Primers for ChIP-qPCR are listed in Table S5. Fold enrichment was determined relative to a negative control, the transposon *TA3*.

Sequencing libraries were prepared from two biological replicates of input and ChIP DNA for stage 6/7 flowers for both *AP1:AP1-GR ap1 cal* and *AP1:AP1-GR ap1 cal ANT:ANT-VENUS ant-4* using Accel-NGS 2S DNA library kit (Swift Biosciences). The libraries were quantitated using the NEBNext Library Quant Kit for Illumina (New England Biolabs) and sequenced on an Illumina HiSeq 2500 producing 150 base paired-end reads. Sequence reads were aligned to the reference *Arabidopsis thaliana* genome (version TAIR9, released June 2009) using bowtie2. Examination of the coverage graphs revealed high reproducibility between the two ChIP-Seq replicates. In addition, the input samples closely resembled the control untagged *AP1:AP1-GR ap1 cal* samples. ANT binding peaks were identified using a visual analytics approach within the Integrated Genome Brower (IGB) (Freese *et al.* 2016). Specifically, coverage graphs were generated for the combined data from the two replicates. A difference coverage graph was generated by subtracting coverage graphs of the untagged sample (*AP1:AP1-GR ap1 cal*) from the coverage graphs for the tagged sample (*AP1:AP1-GR ap1 cal ANT:ANT-VENUS ant-4*). Peaks were defined using the thresholding feature. A thresholding value of 5000 identified 90 peaks while a thresholding value of 1000 identified 11,133 peaks. Further analyses were performed using the 1,113 peaks identified with a threshold value of 1,000. For each identified peak, ChIPpeakAnno was used to identify the gene with the closest transcription start site (TSS) (Zhu *et al.* 2010). GeneOverlap was used to compare gene lists for different ChIP-Seq data sets. Gene Ontology analyses were performed with AmiGO 2 (http://amigo.geneontology.org/amigo). Source code for bioinformatic analyses are available in the project “git” repository https://bitbucket.org/lorainelab/ant-chip/.

Motif analysis with the MEME Suite

Genomic locations of putative ANT binding sites were determined using the FIMO tool of the MEME Suite (Grant *et al.* 2011). The *in vitro* defined ANT binding motif was used as a position specific prior (Nole-Wilson and Krizek 2000). Putative ANT binding sites were

identified using a p value of 0.001 or smaller. *De novo* motif discovery was performed with MEME-ChIP.

Petal measurements

Petal width, length and area were measured as described previously (Krizek 2015).

Accession Numbers

RNA-Seq sequences are available from Sequence Read Archive (https://www.ncbi.nlm.nih.gov/sra) accession number PRJNA539947. ChIP-Seq sequences are available from Sequence Read Archive (https://www.ncbi.nlm.nih.gov/sra) accession number PRJNA593434. Version-controlled source code used to process and analyze data are available from https://bitbucket.org/krizeklab. Sequence alignments and coverage graphs are available for interactive visualization within the Integrated Genome Browser (Nicol *et al.* 2009). To view the data in IGB, readers may download and install the software from https://bioviz.org. Once installed, data sets from the study can be opened within IGB by selecting the latest Arabidopsis thaliana genome and then choosing RNA-Seq and ChIP-Seq folders within the Available Data Sets section of the Data Access Panel.

Supplementary Material

Refer to Web version on PubMed Central for supplementary material.

Acknowledgements

This work was supported by National Science Foundation (NSF) grant IOS 1354452. The Integrated Genome Browser software was supported by National Institutes of Health grants R01-GM103463 and R01-GM121927. Data hosting is provided by the SciDas project, funded by NSF award 1659300 to PI Frank (Alex) Feltus. We thank Roger Deal for helpful suggestions for ChIP experiments and ChIP-Seq library preparation.

References

Aida M, Beis D, Heidstra R, Willemsen V, Blilou I, Galinha C, Nussaume L, Noh Y-S, Amasino R **and** Scheres B (2004) The PLETHORA genes mediate patterning of the Arabidopsis root stem cell niche. Cell, 119, 109–120. [PubMed: 15454085] **and**

Anastasiou E, Kenz S, Gerstung M, MacLean D, Timmer J, Fleck C **and** Lenhard M (2007) Control of plant organ size by KLUH/CYP78A5-dependent intercellular signaling. Dev Cell, 13, 843–856. [PubMed: 18061566] **and**

Azhakanandam S, Nole-Wilson S, Bao F **and** Franks RG (2008) SEUSS and AINTEGUMENTA mediate patterning and ovule initiation during gynoecium medial domain development. Plant Physiol, 146, 1165–1181. [PubMed: 18184731] **and**

Bemis SM **and** Torii KU (2007) Autonomy of cell proliferation and developmental programs during Arabidopsis aboveground organ morphogenesis. Dev Biol, 304, 367–381. [PubMed: 17258192]

Benkova E, Michniewicz M, Sauer M, Teichmann T, Seifertova D, Jurgens G **and** Friml J (2003) Local, efflux-dependent auxin gradients as a common module for plant organ formation. Cell, 115, 591–602. [PubMed: 14651850] **and**

Boutilier K, Offringa R, Sharma VK, Kieft H, Ouellet T, Zhang L, Hattori J, Liu C-M, van Lammeren AAM, Miki BLA, Custers JBM **and** van Lookeren Campagne MM (2002) Ectopic expression of BABY BOOM triggers a conversion from vegetative to embryonic growth. Plant Cell, 14, 1737–1749. [PubMed: 12172019] **and**

Cheng Y, Dai X **and** Zhao Y (2006) Auxin biosynthesis by the YUCCA flavin monooxygenase controls the formation of floral organs and vascular tissues in Arabidopsis. Genes Dev, 20, 1790–1799. [PubMed: 16818609] **and**

Elliott RC, Betzner AS, Huttner E, Oakes MP, Tucker WQJ, Gerentes D, Perez P **and** Smyth DR (1996) AINTEGUMENTA, an APETALA2-like gene of Arabidopsis with pleiotropic roles in ovule development and floral organ growth. Plant Cell, 8, 155–168. [PubMed: 8742707] **and**

Freese NH, Norris DC **and** Loraine AE (2016) Integrated genome browser: visual analytics platform for genomics. Bioinformatics, 32, 2089–2095. [PubMed: 27153568] **and**

Grant CE, Bailey TL **and** Noble WS (2011) FIMO: Scanning for occurrences of a given motif. Bioinformatics, 27, 1017–1018. [PubMed: 21330290] **and**

Heisler MG, Ohno C, Das P, Sieber P, Reddy GV, Long JA **and** Meyerowitz EM (2005) Patterns of auxin transport and gene expression during primodium development revealed by live imaging of the Arabidopsis inflorescence meristem. Curr Biol, 15, 1899–1911. [PubMed: 16271866] **and**

Horstman A, Fukuoka H, Muiño JM, Nitsch L, Guo C, Passarinho P, Sanchez-Perez GF, Immink R, Angenent GC **and** Boutilier K (2015) AIL and HDG proteins act antagonistically to control cell proliferation. Development, 142, 454–464. [PubMed: 25564655] **and**

Huang J, Zhang T, Linstroth L, Tillman Z, Otegui MS, Owen HA **and** Zhao D (2016) Control of anther cell differentiation by the small protein ligand TPD1 and its receptor EMS1 in Arabidopsis. PLoS Genet, 12, e1006147. [PubMed: 27537183] **and**

Hulsen T, de Vlieg J **and** Aikema W (2008) BioVenn-a web application for the comparison and visualization of biological lists using area-proportional Venn diagrams. BMC Genomics, 9, 488. [PubMed: 18925949] **and**

Hyodo H, Yamakawa S, Takeda Y, Tsuduki M, Yokota A, Nishitani K **and** Kohchi T (2003) Active gene expression of a xyloglucan endotransglucosylate/hydrolase gene, XTH9, in inflorescence apices is related to cell elongation in Arabidopsis thaliana. Plant Mol Biol, 52, 473–482. [PubMed: 12856951] **and**

Jofuku KD, den Boer BGW, Van Montagu M **and** Okamuro JK (1994) Control of Arabidopsis flower and seed development by the homeotic gene APETALA2. Plant Cell, 6, 1211–1225. [PubMed: 7919989] **and**

Kaufmann K, Muino JM, Jauregui R, Airoldi CA, Smaczniak C, Krajewski P **and** Angenent GC (2009) Target genes of the MADS transcription factor SEPALLATA3: Integration of developmental and hormonal pathways in the Arabidopsis flower. PLOS Biol, 2009, e1000090.**and**

Kaufmann K, Wellmer F, Muino JM, Ferrier T, Wuest SE, Kumar V, Serrano-Mislata A, Madueno F, Krajewski P, Meyerowitz EM, Angenent GC **and** Riechmann JL (2010) Orchestration of floral initiation by APETALA1. Science, 328, 85–89. [PubMed: 20360106] **and**

Kim EY, Park KY, Seo YS **and** Kim WT (2016) Arabidopsis small rubber particle protein homolog SRPs play dual roles as positive factors for tissue growth and development and in drought stress responses. Plant Physiol, 170, 2494–2510. [PubMed: 26903535] **and**

Kim JH, Choi D **and** Kende H (2003) The AtGRF family of putative transcription factos is involved in leaf and cotyledon growth in Arabidopsis. Plant J, 36, 94–104. [PubMed: 12974814] **and**

Kim JH **and** Kende H (2004) A transcriptional coactivator, AtGIF1, is involved in regulating leaf growth and morphology in Arabidopsis. Proc Natl Acad Sci U S A, 101, 13374–13379. [PubMed: 15326298]

Klucher KM, Chow H, Reiser L **and** Fischer RL (1996) The AINTEGUMENTA gene of Arabidopsis required for ovule and female gametophyte development is related to the floral homeotic gene APETALA2. Plant Cell, 8, 137–153. [PubMed: 8742706] **and**

Krizek BA (1999) Ectopic expression of AINTEGUMENTA in Arabidopsis plants results in increased growth of floral organs. Dev Genet, 25, 224–236. [PubMed: 10528263]

Krizek BA (2009) AINTEGUMENTA and AINTEGUMENTA-LIKE6 act redundantly to regulate Arabidopsis floral growth and patterning. Plant Physiol, 150, 1916–1929. [PubMed: 19542297]

Krizek BA (2015) AINTEGUMENTA-LIKE genes have partly overlapping functions with AINTEGUMENTA but make distinct contributions to Arabidopsis thaliana flower development. J Exp Bot, 66, 4537–4549. [PubMed: 25956884]

Krizek BA, Bequette CJ, Xu K, Blakley I, Fu ZQ, Stratmann JW **and** Loraine AE (2016) RNA-Seq links the transcription factors AINTEGUMENTA and AINTEGUMENTA-LIKE6 to cell wall remodeling and plant defense pathways. Plant Physiol, 171, 2069–2084. [PubMed: 27208279] **and**

Krizek BA **and** Eaddy M (2012) AINTEGUMENTA-LIKE6 regulates cellular differentiation in flowers. Plant Mol Biol, 78, 199–209. [PubMed: 22076630]

Krizek BA **and** Fletcher JC (2005) Molecular mechanisms of flower development: an armchair guide. Nat Rev Genet, 6, 688–698. [PubMed: 16151374]

Lee BH, Wynn AN, Franks RG, Hwang Y. s., Lim J **and** Kim JH (2014) The Arabidopsis thaliana GRF-INTERACTING FACTOR gene family plays an essential role in control of male and female reproductive development. Dev Biol, 386, 12–24. [PubMed: 24355747] **and**

Lee SJ, Lee BH, Jung JH, Park SK, Song JT **and** Kim JH (2018) GROWTH-REGULATING FACTOR and GRF-INTERACTING FACTOR specify meristematic cells of gynoecia and anthers. Plant Physiol, 176, 717–729. [PubMed: 29114079] **and**

Liebsch D **and** Palatnik JF (2020) MicroRNA miR396, GRF transcription factors and GIF co-regulators: a conserved plant organ regulatory module with potential for breeding and biotechnology. Curr Opin Plant Biol, 53, 31–42. [PubMed: 31726426]

Liu Z, Franks RG **and** Klink VP (2000) Regulation of gynoecium marginal tissue formation by LEUNIG and AINTEGUMENTA. Plant Cell, 12, 1879–1891. [PubMed: 11041883] **and**

Machanick P **and** Bailey TL (2011) MEME-ChIP: motif analysis of large DNA datasets. Bioinformatics, 27, 1696–1697. [PubMed: 21486936]

Mandel MA, Gustafson-Brown C, Savidge B **and** Yanofsky MF (1992) Molecular characterization of the Arabidopsis floral homeotic gene APETALA1. Nature, 360, 273–277. [PubMed: 1359429] **and**

Mandel MA **and** Yanofsky MF (1998) The Arabidopsis AGL9 MADS box gene is expressed in young flower primordia. Sex Plant Reprod, 11, 22–28.

Marsch-Martînez N **and** de Folter S (2016) Hormonal control of the development of the gynoecium. Curr Opin Plant Biol, 29, 104–114. [PubMed: 26799132]

Mizukami Y **and** Fischer RL (2000) Plant organ size control: AINTEGUMENTA regulates growth and cell numbers during organogenesis. Proc Natl Acad Sci USA, 97, 942–947. [PubMed: 10639184]

Nicol JW, Helt GA, Blanchard SGJ, Raja A **and** Loraine AE (2009) The Integrated Genome Browser: free software for distribution and exploration of genome-scale datasets. Bioinformatics, 25, 2730–2731. [PubMed: 19654113] **and**

Nole-Wilson S, Azhakanandam S **and** Franks RG (2010) Polar auxin transport together with AINTEGUMENTA and REVOLUTA coordinate early Arabidopsis gynoecium development. Dev Biol, 346, 181–195. [PubMed: 20654611] **and**

Nole-Wilson S **and** Krizek BA (2000) DNA binding properties of the Arabidopsis floral development protein AINTEGUMENTA. Nucleic Acids Res, 28, 4076–4082. [PubMed: 11058102]

Nole-Wilson S **and** Krizek BA (2006) AINTEGUMENTA contributes to organ polarity and regulates growth of lateral organs in combination with YABBY genes. Plant Physiol, 141, 977–987. [PubMed: 16714408]

O'Malley RC, Huang SC, Song L, Lewsey MG, Bartlett A, Nery JR, Galli M, Gallavotti A **and** Ecker JR (2016) Cistrome and epicistrome features shape the regulatory DNA landscape. Cell, 165, 1280–1292. [PubMed: 27203113] **and**

O'Maoiléidigh DS, Thomson B, Raganelli A, Wuest SE, Ryan PT, Kwasniewska K, Carles CC, Graciet E **and** Wellmer F (2015) Gene network analysis of Arabidopsis thaliana flower development through dynamic gene perturbations. Plant J, 83, 344–358. [PubMed: 25990192] **and**

O'Maoiléidigh DS, Wuest SE, Rae L, Raganelli A, Ryan PT, Kwasniewska K, Das P, Lohan AJ, Loftus B, Graciet E **and** Wellmer F (2013) Control of reproductive floral organ identity specification in Arabidopsis by the C function regulator AGAMOUS. Plant Cell, 25, 2482–2503. [PubMed: 23821642] **and**

Pajoro A, Madrigal P, Muiño JM, Matus JT, Jin J, Mecchia MA, Debernardi JM, Palatnik JF, Balazadeh S, Arif M, O'Maoilédigh DS, Wellmer F, Krajewski P, Riechmann JL, Angenent GC **and** Kaufmann K (2014) Dynamics of chromatin accessibility and gene regulation by MADS-

domain transcription factors in flower development. Genome Biol, 15, R41. [PubMed: 24581456] **and**

Prasad K, Grigg SP, Barkoulas M, Yadav RK, Sanchez-Perez GF, Pinon V, Blilou I, Hofhuis H, Dhonukshe P, Galinha C, Mahonen AP, Muller WH, Raman S, Verkleij AJ, Snel B, Reddy GV, Tsiantis M **and** Scheres B (2011) Arabidopsis PLETHORA transcription factors control phyllotaxis. Curr Biol, 21, 1123–1128. [PubMed: 21700457] **and**

Reinhardt D, Eva-Rachele P, Stieger P, Mandel T, Baltensperger K, Bennett M, Traas J, Friml J **and** Kuhlemeier C (2003) Regulation of phyllotaxis by polar auxin transport. Nature, 426, 255–260. [PubMed: 14628043] **and**

Rodriguez RE, Ercoli MF, Debernardi JM, Breakfield NW, Mecchia MA, Sabatini M, Cools T, De Veylder L, Benfey PN **and** Palatnik JF (2015) MicroRNA miR396 regulates the switch between stem cells and transit-amplifying cells in Arabidopsis roots. Plant Cell, 27, 3354–3366. [PubMed: 26645252] **and**

Sabicki S, Arndt D, Marcu A, Lian Y, Grant JR, Maciejewski A **and** Wishart DS (2016) Heatmapper: web-enabled heat mapping for all. Nucleic Acids Res, 44, W147–153. [PubMed: 27190236] **and**

Santuari L, Sanchez-Perez GF, Luijten M, Rutjens B, Terpstra I, Berke L, Gorte M, Prasad K, Bao D, Timmermans-Hereijgers JLPM, Maeo K, Nakamura K, Shimotohno A, Pencik A, Novak O, Ljung K, van Heesch S, de Bruijn E, Cuppen E, Willemsen V, Mähönen AP, Lukowitz W, Snel B, de Ridder D, Scheres B **and** Heidstra R (2016) The PLETHORA gene regulatory network guides growth and cell differentiation in Arabidopsis roots. Plant Cell, 28, 2937–2951. [PubMed: 27920338] **and**

Schiessl K, Muiño JM **and** Sablowski R (2014) Arabidopsis JAGGED links floral organ patterning to tissue growth by repressing Kip-related cell cycle inhibitors. Proc Natl Acad Sci U S A, 111, 2830–2835. [PubMed: 24497510] **and**

Shen L **and** Sinai M (2019) GeneOverlap: Test and visualize gene overlaps. R package version 1220.

Simonini S, Bencivenga S, Trick M **and** Ostergaard L (2017) Auxin-induced modulation of ETTIN activity orchestrates gene expression in Arabidopsis. Plant Cell, 29, 1864–1882. [PubMed: 28804059] **and**

Smaczniak C, Immink RGH, Muino JM, Blanvillain R, Busscher M, Busscher-Lange J, Dinh QD, Liu S, Westphal AH, Boeren S, Parcy F, Xu L, Carles CC, Angenent GC **and** Kaufmann K (2012) Characterization of MADS-domain transcription factor complexes in Arabidopsis flower development. Proc Natl Acad Sci USA, 109, 1560–1565. [PubMed: 22238427] **and**

Stewart D, Graciet E **and** Wellmer F (2016) Molecular and regulatory mechanisms controlling floral organ development. FEBS J, 283, 1823–1830. [PubMed: 26725470] **and**

Unte US, Sorensen A-M, Pesaresi P, Gandikota M, Leister D, Saedler H **and** Huijser P (2003) SPL8, an SBP-Box gene that affects pollen sac development in Arabidopsis. Plant Cell, 15, 1009–1019. [PubMed: 12671094] **and**

Winter CM, Austin RS, Blanvillain-Baufumé S, Reback MA, Monniaux M, Wu M-F, Sang Y, Yamaguchi A, Yamaguchi N, Parker JE, Parcy F, Jensen ST, Li H **and** Wagner D (2011) LEAFY target genes reveal floral regulatory logic, cis motifs, and a link to biotic stimulus response. Dev Cell, 20, 430–443. [PubMed: 21497757] **and**

Wuest SE, O'Maoiléidigh DS, Rae L, Kwasniewska K, Raganelli A, Hanczaryk K, Lohan AJ, Loftus B, Graciet E **and** Wellmer F (2012) Molecular basis for the specification of floral organs by APETALA3 and PISTILLATA. Proc Natl Acad Sci USA, 109, 13452–13457. [PubMed: 22847437] **and**

Xiao J, Jin R, Yu X, Shen M, Wagner JD, Pai A, Song C, Zhuang M, Klasfeld S, He C, Santos AM, Helliwell C, Pruneda-Paz JL, Kay SA, Lin X, Cui S, Garcia MF, Clarenz O, Goodrich J, Zhang X, Austin RS, Bonasio R **and** Wagner D (2017) Cis and trans determinants of epigenetic silencing by Polycomb repressive comples 2 in Arabidopsis. Nat Genet, 49, 1546–1552. [PubMed: 28825728] **and**

Xing S, Salinas M, Höhmann S, Berndtgen R **and** Huijser P (2010) miR156-targeted and nontargeted SBP-box transcription factors act in concert to secure male fertility in Arabidopsis. Plant Cell, 22, 3935–3950. [PubMed: 21177480] **and**

Yamaguchi N, Winter CM, Wu M-F, Kwon CS, William DA **and** Wagner D (2014) Chromatin Immunoprecipitation from Arabidopsis tissue. The Arabidopsis Book, e0170.**and**

Yamaguchi N, Wu M-F, Winter CM, Berns MC, Nole-Wilson S, Yamaguchi A, Coupland G, Krizek BA **and** Wagner D (2013) A molecular framework for auxin-mediated initiation of flower primordia. Dev Cell, 24, 271–282. [PubMed: 23375585] **and**

Yamaguchi T, Nukazuka A **and** Tsukaya H (2012) Leaf adaxial-abaxial polarity specification and lamina outgrowth: evolution and development. Plant Cell Physiol, 53, 1180–1194. [PubMed: 22619472] **and**

Yan W, Chen D **and** Kaufmann K (2016) Molecular mechanisms of floral organ specification by MADS domain proteins. Curr Opin Plant Biol, 29, 154–162. [PubMed: 26802807] **and**

Zhao DZ, Wang GF, Speal B **and** Ma H (2002) The EXCESS MICROSPOROCYTES1 gene encodes a putative leucine-rich repeat receptor protein kinase that controls somatic and reproductive cell fares in the Arabidopsis anther. Genes Dev, 16, 2021–2031. [PubMed: 12154130] **and**

Zhu LJ, Gazin C, Lawson ND, Pagés H, LIn SM, Lapointe DS **and** Green MR (2010) ChIPpeakAnno: a Bioconductor package to annotate ChIP-seq and ChIP-chip data. BMC Bioinformatics, 11, 237. [PubMed: 20459804] **and**

Zúñiga-Mayo VM, Gómez-Felipe A, Herrera-Ubaldo H **and** de Folter S (2019) Gynoecium development: networks in Arabidopsis and beyond. J Exp Bot, 70, 1447–1460. [PubMed: 30715461] **and**

Significance Statement

"Flower development has been extensively studied, but our knowledge of gene regulatory networks generating floral organs with characteristic forms remains incomplete. This study used a highly targeted genomic approach to identify 200 genes likely to be direct targets of regulation by AINTEGUMENTA (ANT), a transcription factor regulating flower patterning and growth. Our set of identified target genes include those with known roles in polarity specification, floral organ development, lateral organ growth, and auxin signaling."

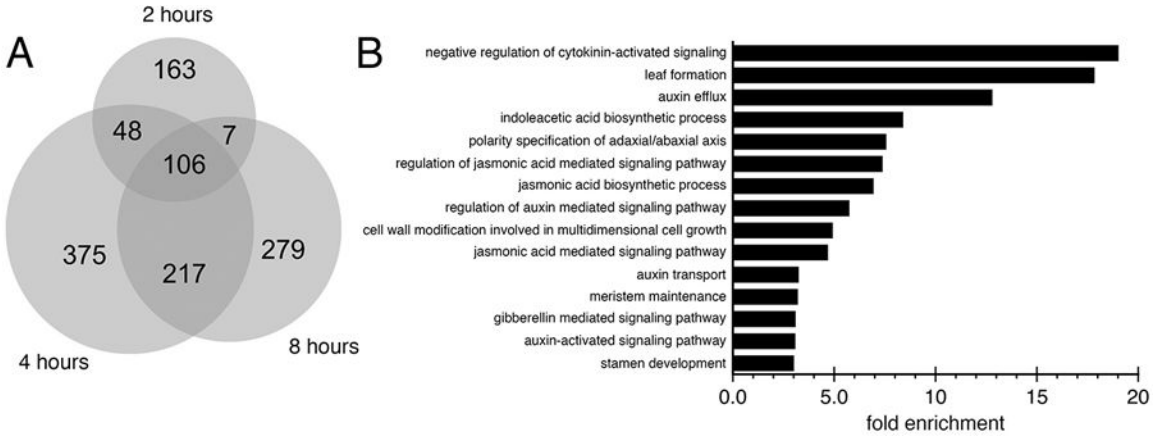

Figure 1. Genes differentially expressed (DE) in mock and dex treated *35S:ANT-GR* inflorescences.

A. Venn diagram showing overlap between DE genes identified at two, four and eight hours after treatment. The Venn diagram was created with BioVenn (Hulsen *et al.* 2008). B. Biological process GO terms enriched in DE genes.

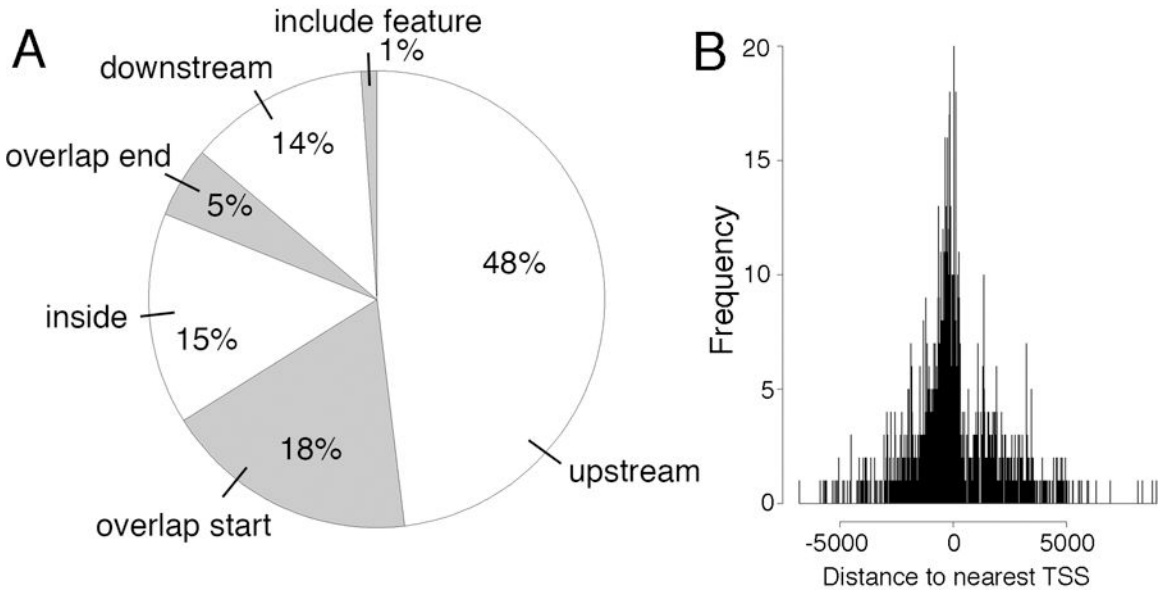

Figure 2. Position of ANT ChIP-Seq peaks relative to closest gene.

A. Pie chart showing the position of ANT ChIP-Seq binding peaks relative to the closest gene. Almost half of the peaks are upstream of the closest gene (48%). The remaining peaks either overlap the start of the gene (18.0%), are within the gene (15%), overlap the end of the gene (5%), are downstream of the gene (14%) or overlap the entire gene (1%). B. Position of ANT binding peak relative to the transcriptional start site (TSS) of the closest gene.

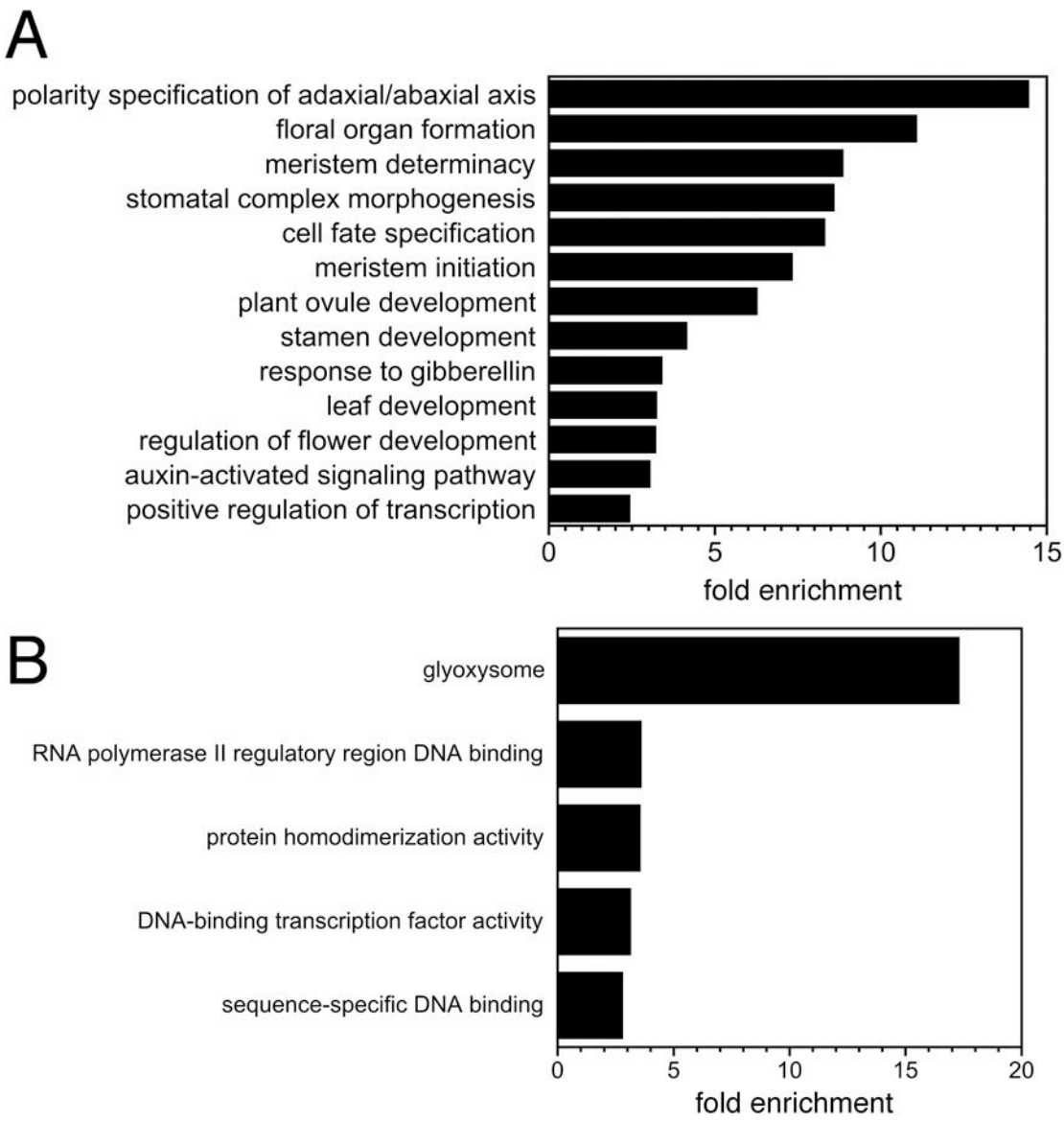

Figure 3. GO enrichment analyses on genes associated with ANT ChIP-Seq binding peaks

A. Biological process GO terms enriched in genes associated with ANT binding peaks. B. Molecular function and cellular component GO terms enriched in genes associated with ANT binding peaks.

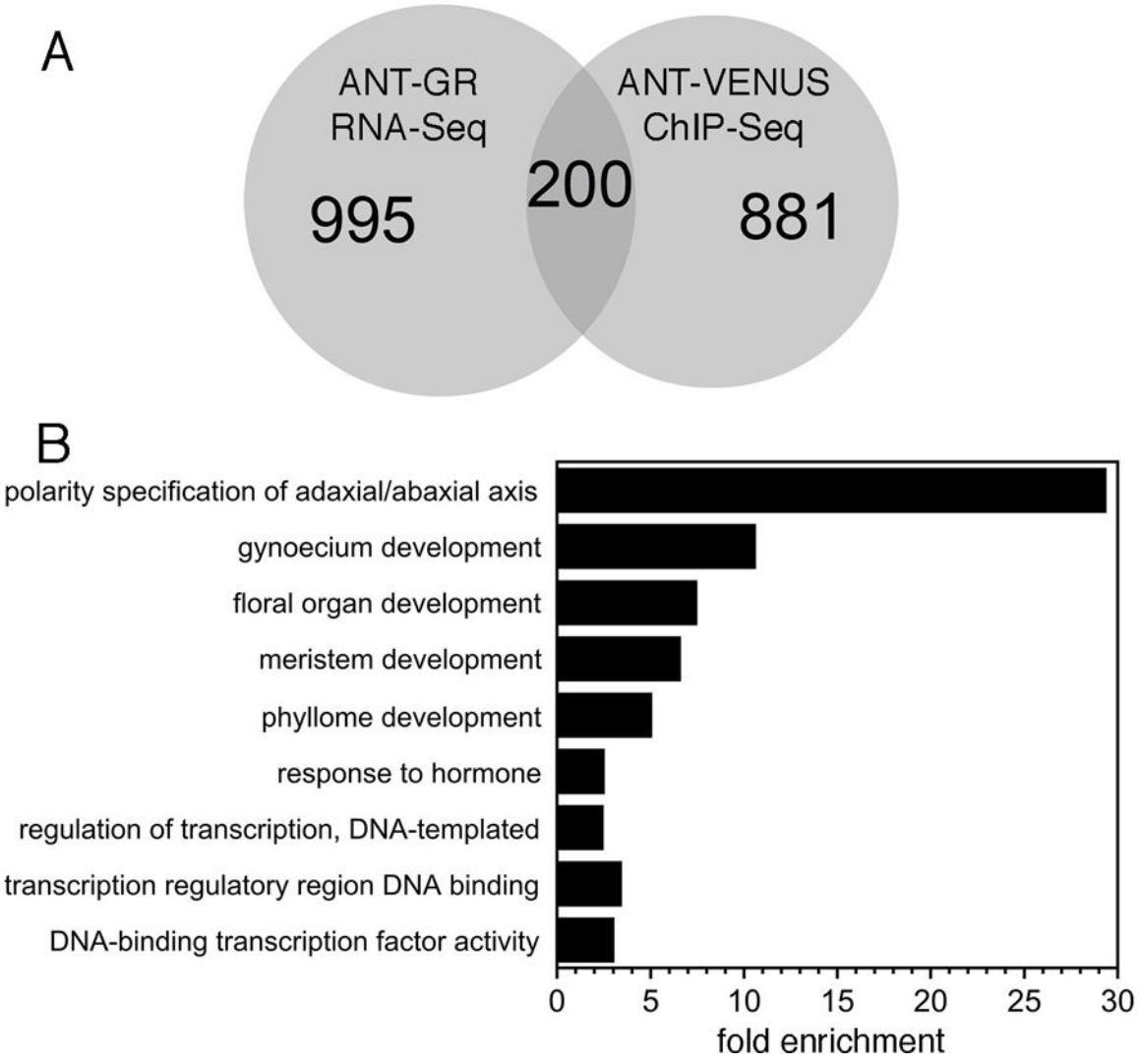

Figure 4. DE genes that are bound by ANT.

A. Venn diagram showing overlap between DE genes identified and those bound by ANT. The Venn diagram was created with BioVenn (Hulsen *et al.* 2008). B. Biological process and molecular function GO terms enriched in genes that are both DE and bound by ANT.

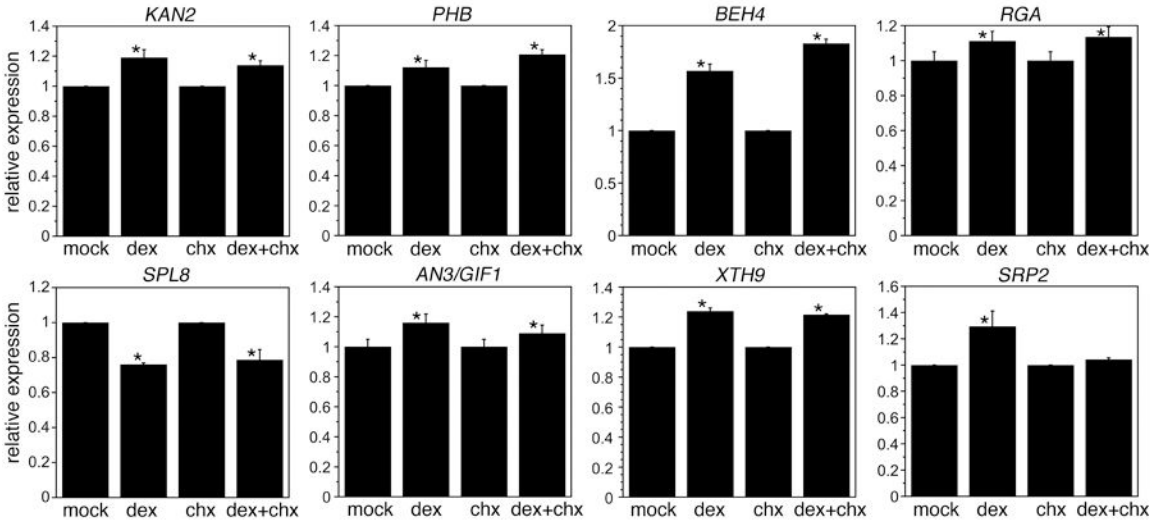

Figure 5. Several tested DE genes show protein synthesis independent gene expression changes after induction of ANT activity in *35S:ANT-GR*.

Graphs show relative expression of *KAN2, PHB*, *BEH4, RGA, SPL8*, *AN3/GIF1*, *XTH9*, and *SRP2* after mock, dexamethasone (dex), cycloheximide (chx), dex+chx treatments. Relative expression refers to mRNA levels in dex samples compared to mock samples and mRNA levels in dex+chx samples compared to chx samples. * indicates dex samples statistically different than mock samples and dex+chx samples statistically different than chx samples as determined by Students *t*-test (*P* value less than 0.05). mRNA levels were measured 4 hours after treatment. Graphs show mean ± SD of two biological replicates.

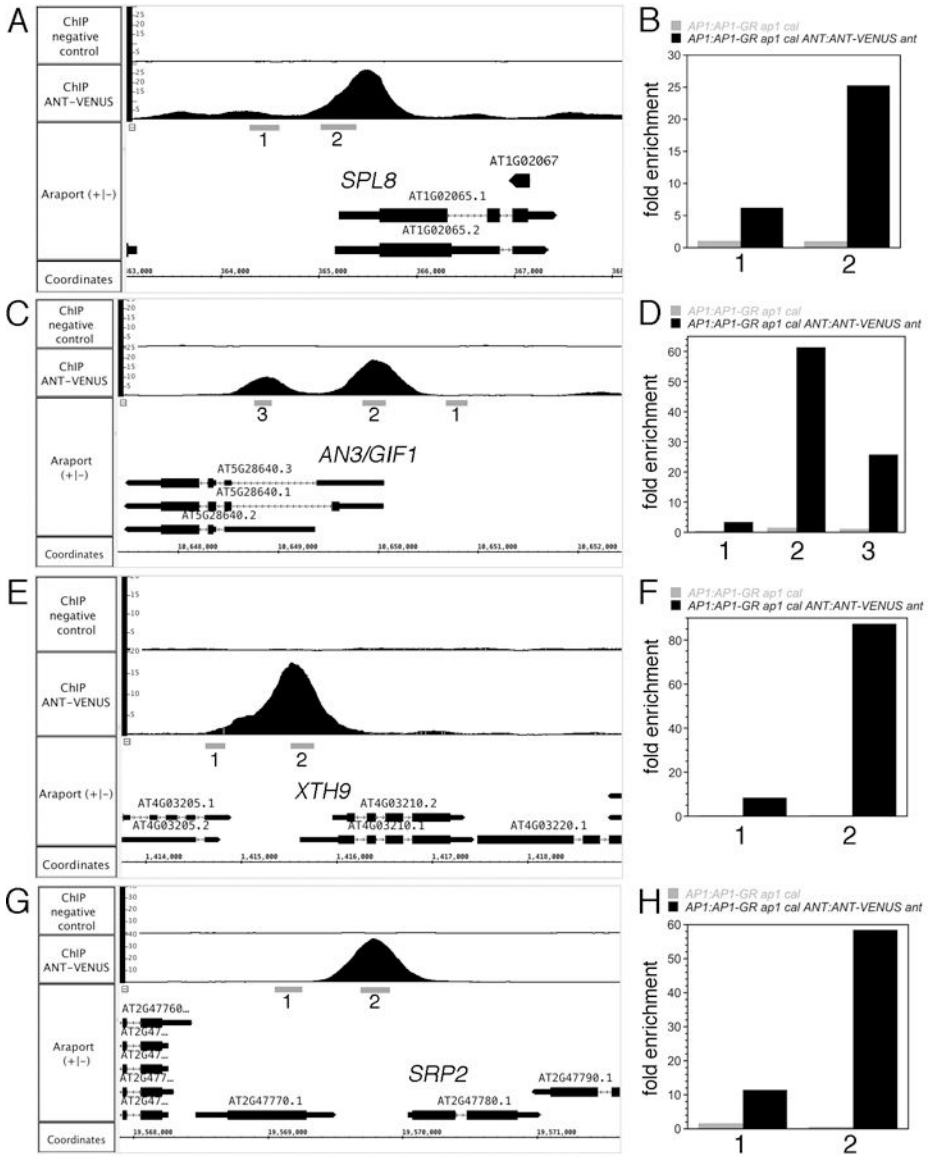

Figure 6. ChIP-qPCR confirms that ANT binds to genomic regions upstream or within genes associated with stamen development (*SPL8*) and growth (*AN3/GIF1, XTH9, SRP2*).

ChIP-Seq coverage graphs for *SPL8* (A), *AN3/GIF1* (B), *XTH9* (E), and *SRP2* (G). Numbers below the gene indicate the regions tested for ANT binding by ChIP-qPCR. ChIP-qPCR data for *SPL8* (B), *AN3/GIF1* (D), *XTH9* (F) and *SRP2* (H). Grey bars show results from *AP1:AP1-GR ap1 cal* and black bars show results from *AP1:AP1-GR ap1 cal ANT:ANT-VENUS ant*. Numbers on the x axis correspond to the genomic regions indicated in the ChIP-Seq coverage graphs.

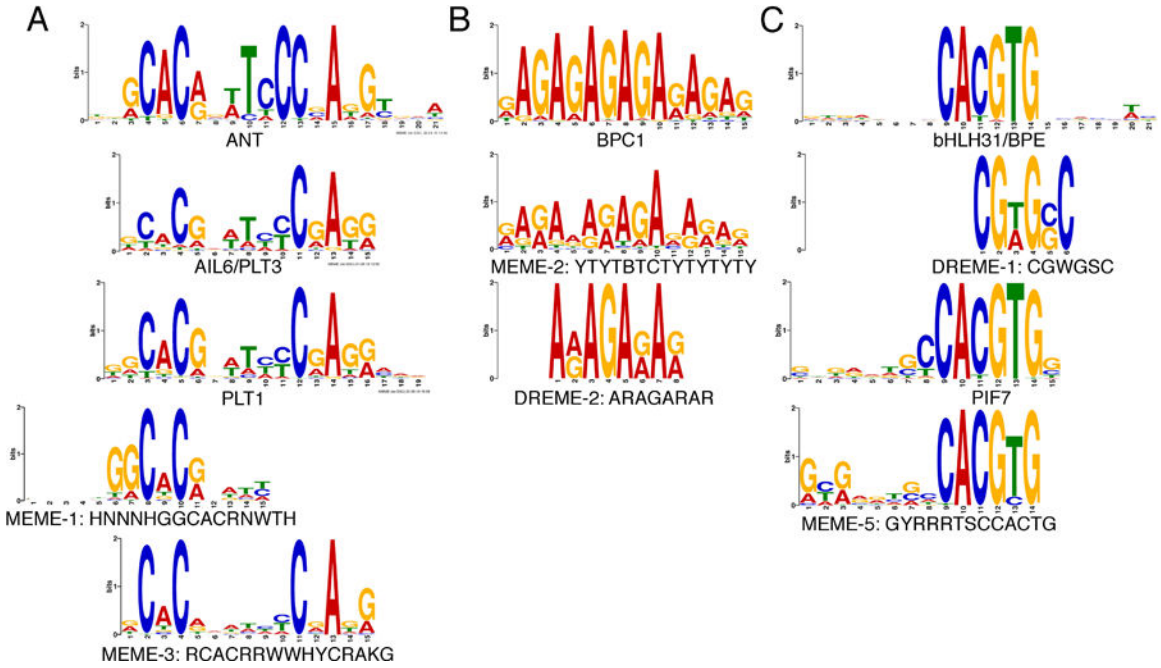

Figure 7. MEME-ChIP identifies sequences with similarity to AIL/PLT sites as well as other transcription factors.

A. Sequence logos representing the DNA binding specificities of ANT, AIL6/PLT3, PLT1 and two motifs (MEME-1 and MEME-3) identified within ANT ChIP-Seq binding peaks. B. Sequence logos representing the DNA binding specificity of BPC1 and two related motifs (MEME-2, DREME-2) identified within ANT ChIP-Seq binding peaks. C. Two bHLH binding sites from bHLH31/BPE and PIF7 and two related motifs (DREME-1 and MEME-5) identified within ANT ChIP-Seq binding peaks.

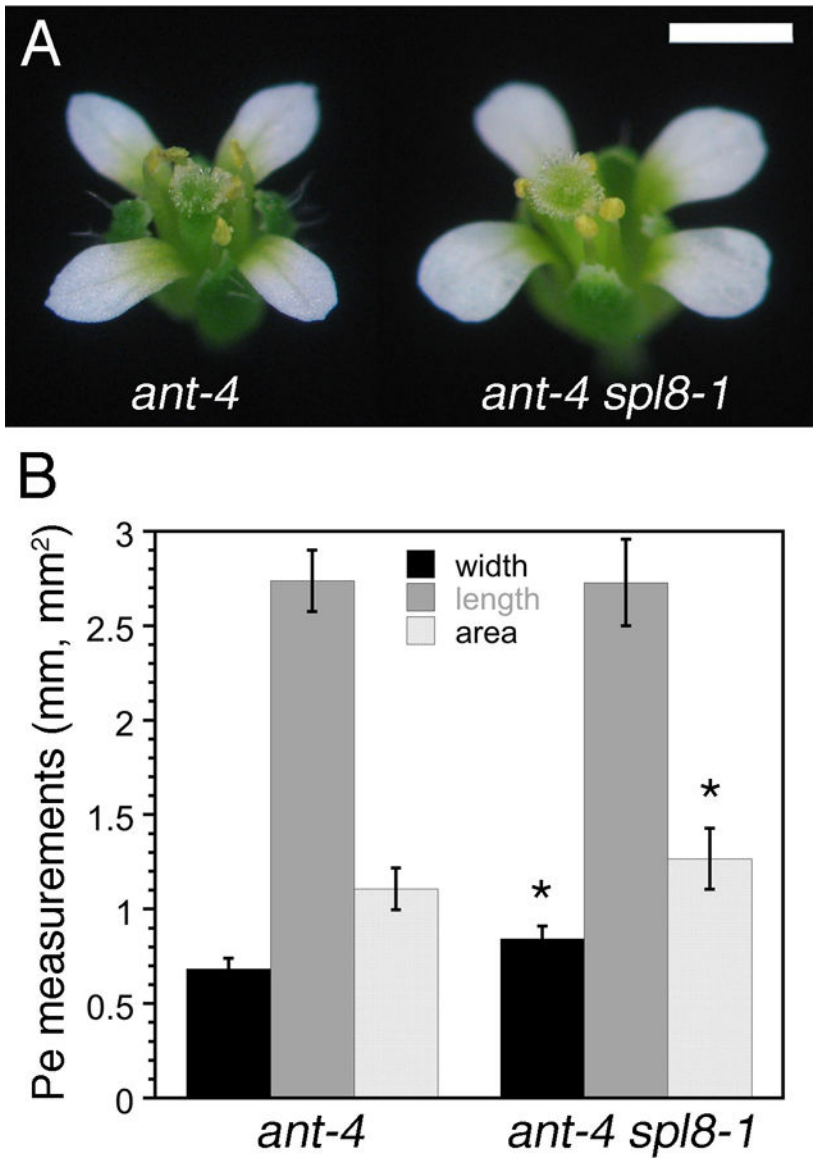

Figure 8. Mutations in *SPL8* partially rescue the petal size defects of *ant* flowers.

A. *ant-4* flower (left) and *ant-4 spl8–1* flower (right). B. Petal width, length and area in *ant-4* and *ant-4 spl8–1* flowers. * indicates values with a *P* value less than 0.05 (Student's *t*-test). Size bar is 1mm.

Table 1.

Developmental genes DE after ANT-GR activation and bound by ANT

Polarity specification	**Name**	**log2 fold change (hr)**	**ChIP-Seq**
AT2G34710	*PHB*	0.256 (4); 0.346 (8)	upstream; overlap start
AT3G57130	*BOP1*	−0.449 (4)	upstream
AT2G37630	*AS1*	−0.235 (4); −0.175 (8)	upstream
AT1G32240	*KAN2*	0.227 (4); 0.255 (8)	inside
AT4G00180	*YAB3*	0.269 (2); 0.262 (4); 0.374 (8)	upstream
Floral organ development			
AT1G69120	*AP1*	−0.144 (4)	upstream; overlap start
AT4G36920	*AP2*	0.22 (2)	upstream
AT1G24260	*SEP3*	0.175 (8)	inside
AT1G02065	*SPL8*	−0.341 (2); −0.589 (4); −0.534 (8)	overlap start
AT5G07280	*EMS1*	−0.14 (4)	upstream
AT1G11130	*SUB*	0.154 (4); 0.165 (8)	overlap start
AT4G36930	*SPT*	0.269 (2); 0.297 (4); 0.418 (8)	upstream
Growth genes			
AT1G13710	*KLU/CYP78A5*	−0.281 (2); −0.272 (4)	upstream
AT4G24150	*GRF8*	0.317 (8)	inside
AT5G28640	*AN3/GIF1*	0.244 (2); 0.25 (4); 0.403 (8)	overlap start, inside
AT4G03210	*XTH9*	0.315 (2); 0.351 (4); 0.405 (8)	upstream
AT2G47780	*SRP2*	0.482 (4); 0.718 (8)	overlap start
AT2G32710	*KRP4*	0.293 (2); 0.299 (4); 0.331 (8)	overlap end

Table 2.

Hormone genes DE after ANT-GR activation and bound by ANT

AGI locus code	Gene	log2 fold change (hr)	ChIP-Seq
Auxin			
AT1G70560	*TAA1/WEI8*	0.297 (4); 0.444 (8)	inside
AT3G26810	*AFB2*	0.185 (8)	upstream
AT1G30330	*ARF6*	0.132 (4)	upstream
AT2G46530	*ARF11*	0.376 (8)	upstream
AT3G61830	*ARF18*	0.198 (8)	overlap end
AT1G04240	*SHY2/IAA3*	0.285 (8)	overlap start
AT4G29080	*PAP2/IAA27*	0.14 (4)	upstream
AT4G34760	*SAUR50*	0.346 (8)	upstream
AT4G38840	*SAUR14*	−0.478 (4)	overlap start
Gibberellin			
AT1G14920	*GAI*	0.133 (4); 0.181 (8)	upstream
AT2G01570	*RGA*	0.246 (2); 0.259 (4); 0.334 (8)	upstream
Brassinosteroid			
AT1G78700	*BEH4*	0.664 (2); 0.734 (4); 0.918 (8)	inside
Abscisic Acid			
AT2G40330	*PYL6*	0.552 (2)	overlap start
Ethylene			
AT1G15360	*WIN1/SHN1*	−0.212 (8)	overlap start

Table 3.

MEME-ChIP analysis of ANT ChIP-Seq peaks

Motif	Motif ID	Width	Sites	e-value	Most similar motif
HNNNHGGCACRNWTH	MEME-1	15	267	5.80E-251	PLT1 (AP2/ERF)
YTYTBTCTYTYTYTY	MEME-2	15	400	2.00E-169	BPC5 (BBR/BPC)
RCACRRWWHYCRAKG	MEME-3	15	263	7.30E-99	AIL6/PLT3 (AP2/ERF)
CGWGSC	DREME-1	6	221	8.70E-19	BPE/bHLH31 (bHLH)
ARAGARAR	DREME-2	8	348	5.30E-16	BPC1 (BBR/BPC)
AAARGHRGARARARAAADARAAVAAMAAA	MEME-4	29	64	2.60E-15	VRN1 (ABI3/VP1)
GYRRRTSCCACGTG	MEME-5	14	39	8.30E-11	PIF7 (bHLH)